A&A 442, 757–766 (2005)
DOI: 10.1051/0004-6361:20040559

Astronomy & Astrophysics

Electron-ion recombination of Be-like C, N, and O

M. Fogle[1] ⋆, N. R. Badnell[2], P. Glans[3], S. D. Loch[4], S. Madzunkov[1], Sh. A. Abdel-Naby[4], M. S. Pindzola[4], and R. Schuch[1]

[1] Department of Physics, AlbaNova University Center, Stockholm University, SE106 91 Stockholm, Sweden
[2] Department of Physics, University of Strathclyde, Glasgow G4 0NG, UK
[3] Department of Engineering, Physics, and Mathematics, Mid-Sweden University, SE851 70 Sundsvall, Sweden
[4] Department of Physics, Auburn University, Auburn, Alabama 36849, USA

Received 30 March 2005 / Accepted 1 July 2005

ABSTRACT

The absolute total recombination reaction rate coefficients for Be-like C, N, and O have been measured using the CRYRING storage ring and compared with the results from distorted-wave theory. For the theory results, it is found that shifts to NIST energy values for the core excited energies of the recombining system are not sufficient to accurately match all of the resonance positions and heights at lower energies. These theory results represent the quality of most archived theory DR data. The accurate calculation of these low energy resonances still presents a significant challenge to theory. In addition, trielectronic recombination resonances, associated with the formation of triply excited states during recombination, have been observed in the total recombination reaction rate coefficient spectra of N^{3+} and O^{4+}. Finally, we construct a dielectronic recombination Maxwellian rate coefficient from the experimental results for low n resonances, and from the theoretical results for high n resonances. In the case of O^{4+}, the trielectronic recombination resonances have a strong influence on the low temperature Maxwellian rate coefficient. Our best hybrid Maxwellian rate coefficient is compared with archived distorted-wave theory data, and is found to be in reasonable agreement, even at the low temperatures.

Key words. atomic – molecular and nuclear data

1. Introduction

Being among the most abundant elements in the universe, carbon, nitrogen, and oxygen emanate in a wide range of observations. The electron-ion recombination processes (Schuch 1993) undergone by ions of these elements lead to the emission of satellite recombination lines used extensively for plasma diagnostics, such as in electron temperature and elemental abundance determinations. In fact, there is a longstanding enigma related to the determination of elemental abundances via collisionally excited lines (CELs) and optical recombination lines (ORLs) (Kaler 1981; Kholtygin & Feklistova 1992; Liu 2002). In planetary nebulae, the typical phenomenon observed is that the abundances deduced from CELs are up to 20 times less than those deduced from ORLs. CELs are readily observed in emission spectra, due to the transpicuous nature of the plasma at stabilization photon energies, while ORLs experience a large opacity and are usually much less intense; leading to poor signal-to-noise ratios which restrict accurate measurements. With the advent of high resolution spectrometers, particularly space-based, this unresolved issue has regained attention and explanations ranging from poor atomic data to plasma inhomogeneities have been offered.

The first experimental total recombination reaction rate coefficient measurements of Be-like C, N, and O were made by Dittner et al. (1987). The resolution of these experiments was poor; in that no discernable resonance structure was observed in the spectra. The influence of core fine-structure interaction on dielectronic recombination (DR) in Be-like C, N and O were studied by Badnell (1988). Higher resolution measurements of Be-like C and O were reported by Badnell et al. (1991). The contributions from the metastable $2s2p\ ^3P$ state were more prominent in these experiments and were discussed in detail. Neither of these previous measurements, however, provided a detailed measurement of the region just a few eV above threshold, due to their lack of resolution and experimental limitations. This low energy region can be rich in resonances of significant strength, leading to a profound impact on the low temperature plasma recombination rate coefficients and the ionization equilibrium for photoionized plasmas derived from these rates.

Dielectronic recombination involves forming doubly excited states which radiatively stabilize below the autoionization threshold. This, however, is not the only resonant recombination process to consider. A recent publication by Schnell et al. (2003) discussed the first observation of resonant recombination via triply excited states; *trielectronic recombination* (TR). For Be-like ions, this entails the recombination of an electron to an nl state and the simultaneous excitation of the $2s^2$ ground state to $2p^2$. Trielectronic recombination resonances which lie close to threshold can contribute significantly to the low energy region of the spectrum, since the strength of a given resonance is inversely proportional to the incident

⋆ *Present address:* Physics Division, Oak Ridge National Laboratory, Oak Ridge, TN 37831-6372.

electron energy. Such triply excited states can also have radiative rates comparable to the autoionization rates, and it is the magnitude of the lesser quantity which contributes to the resonance strength. Such strong resonances will dramatically effect the low temperature region of the corresponding plasma rate coefficient; e.g., in O^{4+}.

Ion storage rings coupled with electron coolers represent a paradigm in total recombination reaction rate coefficient measurements, setting the standard for combined energy and rate resolution. Over the past couple of decades, it has been these machines which have been at the forefront in experimental rate coefficient measurements, covering a vast array of ion species (Müller & Wolf 1997; Schippers 1999). The electron cooler, used to reduce the stored ion beam's emittance and momentum dispersion, doubles as the electron target in recombination experiments. The electron cooler at CRYRING, for example, is capable of providing longitudinal center-of-mass (CM) collision energies down to $\sim 100\,\mu$eV, facilitating the detailed study of both nonresonant radiative recombination (RR) and resonant recombination processes. Here we present experimental recombination rate coefficients for the Be-like ions C^{2+}, N^{3+}, and O^{4+} obtained using the synchrotron storage ring CRYRING. All observed resonances are of the $\Delta n = 0$ type. The resulting experimental rate coefficients are adjusted for field ionization, which leads to an n-cutoff above which recombined ions are re-ionized and go undetected. They are then convoluted with Maxwellian temperature distributions to produce temperature-dependent plasma recombination rate coefficients. These plasma rate coefficients are compared to those from recent calculations of Colgan et al. (2004b), to some more complex calculations, and to some results from literature.

2. Experiment

The experiments discussed here were performed at the heavy ion storage ring CRYRING. The Be-like ions C^{2+}, N^{3+}, and O^{4+} were produced by an electron cyclotron resonance (ECR) ion source of the hypernanogan type operated at a fixed RF frequency of 14.5 GHz and RF powers of 180, 130, and 400 W, respectively. The ions were injected into the ring and accelerated to maximum energy, as defined by the magnetic rigidity of 1.44 T m. The respective final energies for C^{2+}, N^{3+}, and O^{4+} were 2.7 MeV/amu, 4.4 MeV/amu, and 6.0 MeV/amu, and the initial stored ion currents were 470 nA, 536 nA, and 90 nA, respectively. The ions were cooled with the electron cooler coupled to the ring by velocity matching the electrons and ions. This resulted in a cooled ion beam with a diameter of approximately 1 mm. The electron beam was adiabatically expanded, from the cathode to the interaction region, a factor of twenty-five times giving a final electron beam diameter of 2 cm. This provided a flattened Maxwellian electron temperature (k_BT) distribution characterized by a transverse temperature of $k_BT_\perp = 4$ meV and a longitudinal temperature of $k_BT_\parallel = 0.1$ meV, with respect to the ion beam direction. The electron densities in the interaction region were approximately 3×10^7 cm^{-3}.

At the velocity matched cooling condition, RR is the dominate recombination channel. In order to investigate resonant DR (and TR) processes, the electron velocity is systematically varied over selected CM energy ranges. Charge changed ions were separated from the stored beam by the dipole magnet following the electron cooler and detected by a unity efficiency surface barrier detector as a function of the varied electron cooler cathode potential. Further details on the experimental technique are discussed by DeWitt et al. (1996) and Zong et al. (1997).

Systematic corrections for the electron beam space charge and the drag force exerted on the ion beam, by the electron beam, are taken as described in the references above. The error in the measured CM energies is estimated at 10 meV, which is derived primarily from the uncertainties in the cathode voltage measurement and the drag force correction. The predominate uncertainties in the measured rate coefficients arise from the determination of the ion current (~15%) and the uncertainty of the electron-ion interaction length (~5%).

The ion beam metastable fractions for C^{2+}, N^{3+}, and O^{4+} were estimated to be 60%, 40%, and 35%, respectively. We will assume here that the majority of the metastable fraction is due to the population of the 2s2p $^3P_0$ state whose lifetime is extremely large (calculated as $\sim 10^{10}$ s for C^{2+} by Laughlin 1980), and thus goes unchanged during any experimental measuring window. If it were not for the metastable presence in the experiment, we would produce total DR rate coefficients by simply using AUTOSTRUCTURE to extrapolate the n-cutoff series limits from our experimental results. As things stand, it is not possible to produce an experimental total DR rate coefficient without having to separate the contributions from the ground and metastable levels. Our method for doing this is discussed in the Results and Discussion section.

3. Theory

We use the AUTOSTRUCTURE code (Badnell 1986) to evaluate the level energies, Auger and radiative rates necessary to calculate the dielectronic recombination rate coefficients. This method has been used frequently in the past, and has been found to provide good agreement with resonance position for Rydberg series, especially for the higher n-shell resonances. Recently, the AUTOSTRUCTURE code has been used as part of a project aimed at calculating comprehensive DR data for complete isoelectronic sequences; see Badnell et al. (2003). Results have been published on Li-like (Colgan et al. 2004a), Be-like (Colgan et al. 2004b), B-like (Altun et al. 2004), C-like (Zatsarinny et al. 2004a), N-like (Mitnik et al. 2004), O-like (Zatsarinny at al. 2003), Ne-like (Zatsarinny at al. 2004b), and calculations are underway for other isoelectronic sequences. In these datasets, all calculations are ab-initio, with the exception that core excited energies of the recombined system have been shifted to energy values list in the NIST levels database, where available. Typical energy shifts for the AUTOSTRUCTURE calculation of this paper are approximately 0.02 eV for all core excited energies, with the exception of the 2s2p ^{1}P, 2p^2 ^{1}D, and ^{1}S terms, which have shifts close to 1 eV. Applying such a shift for the low-n resonances does not always lead to good resonance positions for the low energy resonances (mostly $n = 3$ and $n = 4$ resonances in our case). This level of

calculation is representative of the quality of data in most DR databases. Thus, the AUTOSTRUCTURE data which we show in this paper, with the core excited energy shifts applied, will be referred to as our "default" AUTOSTRUCTURE calculation. This default calculation consists of $1s^22s^2nl$, $1s^22s2pnl$, $1s^22p^2nl$, $1s^22s^22p$, $1s^22s2p^2$, $1s^22p^3$ and continuum configurations, where the nl values loop over a range of values from $n = 3$ up to the n-cutoff.

In order to see if we can achieve better agreement with the low energy resonance positions and heights, we consider two alternative theory approaches. In the first case, core excited energy shifts are not included, and an AUTOSTRUCTURE calculation is performed with many configurations included explicitly, to include as much configuration interaction as possible. We note that these low energy resonances are only slowly converging with configuration interaction effects. In all of the cases discussed here, the following configurations were included explicitly: $2s^2nl$, $2s2pnl$, $2p^2nl$ ($n = 3 \rightarrow 8$), $2s^22p$, $2s2p^2$ and $2p^3$. If this did not give improved results, we took the large configuration interaction calculation and shifted all of the $n = 3$ and 4 resonance positions to NIST energy values.

We also calculate what we will refer to as a "hybrid" Maxwellian DR rate coefficient. Here we take the experimental resonance resolved measurements, and separate the resonances coming from an initial ground configuration with those coming from the metastable level. This is done with the guidance of the AUTOSTRUCTURE calculation, and using NIST resonance energies where available. We then "top up" the experimental results with AUTOSTRUCTURE data for resonances above the n-cutoff. There is some uncertainty in this method, mostly due to uncertainties in determining which low energy resonances are attached to the ground level, and which to the metastable level. In our cases, using NIST energy values, we were able to identify most of the resonance positions in question. Thus, differences between the Maxwellian DR rate coefficients produced in this hybrid calculation with that from our default AUTOSTRUCTURE calculation will give an indication of the likely uncertainties in the existing DR databases.

4. Results and discussion

4.1. $C^{2+} + e^- \rightarrow C^+$

The experimental total recombination reaction rate coefficient is shown in Fig. 1 along with energy positions for the $2s^2\,{}^1S \rightarrow 2s2p(^1P)nl$, $2s^2\,{}^1S \rightarrow 2s2p(^3P)nl$, and $2s2p\,{}^3P \rightarrow 2s2p(^1P)nl$ series limits given by

$$E = E_s - \frac{RZ^2}{n^2}\,, \tag{1}$$

where E_s is the respective energy splitting over which the bound electron is excited during recombination, R is the mass reduced Rydberg constant, Z is the effective charge, and n is the principal quantum state where the incoming electron recombines. For C^{2+}, the respective values for E_s are 12.7, 6.5, and 6.2 eV. The Rydberg series, depicted as vertical bars on the figures for all of the ions discussed here, begin with the lowest n and range up to the n-cutoff. The lowest principal quantum state for which DR is possible for all of these series in C^{2+} is $n = 3$. The upper limit for the experimentally observed principal quantum state is governed by field ionization of the recombined electron. In the flight path from the electron cooler to the detector, the motional electric field induced in various magnetic elements of the ring can be large enough to re-ionize the recombined ion. This leads to an n-cutoff above which all other recombined states will be ionized. This n-cutoff is given by

$$n_{\rm cutoff} \simeq \left(6.2 \times 10^{10}\,\frac{Q^3}{v_{\rm i}\,B}\right)^{1/4}\,, \tag{2}$$

where Q is the ion charge, $v_{\rm i}$ is the stored ion velocity,and B is the magnetic field strength (T). The most dramatic n-cutoff is found in the main dipole magnetic which separates the charge changed ions from the stored beam. Given the storage velocity for C^{2+} and the dipole field strength of 1.2 T, Eq. (2) yields an n-cutoff of 12. This cutoff value does not take into account the time of flight from the electron cooler to the magnet. During this time, a recombined electron could decay below the n-cutoff and survive passage through the magnet. This is clearly seen in the experimental rate coefficient at the $^1S - {}^1P$ series limit, shown in Fig. 1, where a shoulder appears above the calculated n-cutoff. In our default AUTOSTRUCTURE calculation we include a time-of-flight option (equal to 100 ns) in our comparison with the resonance resolved results of the experiment. This accounts for electrons which have recombined above the n-cutoff and decay, to a state which will survive the field, during the time-of-flight from the electron cooler to the magnet. A detailed analysis of field ionization and survival probabilities in storage ring experiments is given by Schippers et al. (2001).

In Fig. 1 we show the experimental results along with two AUTOSTRUCTURE results. One AUTOSTRUCTURE result shows the calculation including the core excited energy shifts to NIST values (unshaded results in plots 2 and 4), this represents the standard quality of theoretical data in most DR databases, e.g., Colgan et al. (2004b). The second AUTOSTRUCTURE results shown (shaded results in plots 2 and 4) are from the large configuration interaction calculation we performed and are for the $n = 3$ and 4 resonances only. It can be seen that the default AUTOSTRUCTURE calculation does very well for resonances from $n = 5$ up to the n-cutoff. There are clearly differences in the low energy positions and heights, even using our large configuration interaction results. We also attempted to artificially shift our AUTOSTRUCTURE resonance positions to NIST energy values for this large configuration interaction calculation, however, we achieved no improvement in the low energy resonances heights and so these results are not shown on the plots.

The experimental RR rate coefficient is given in Fig. 2. As can be seen in the figure, the RR rate falls off rapidly with increasing energy and in the region $E \rightarrow 0$, the RR rate is enhanced. This enhancement is a phenomenon typically observed in storage ring measurements, see Gao et al. (1995), and is the subject of ongoing studies. The RR rate coefficient to a specific principal quantum state is given by

$$\alpha_n^{\rm RR} = \int \sigma_n^{\rm RR}(E\,(v))\;v\,f(\hat{v},\boldsymbol{v})\,{\rm d}^3v, \tag{3}$$

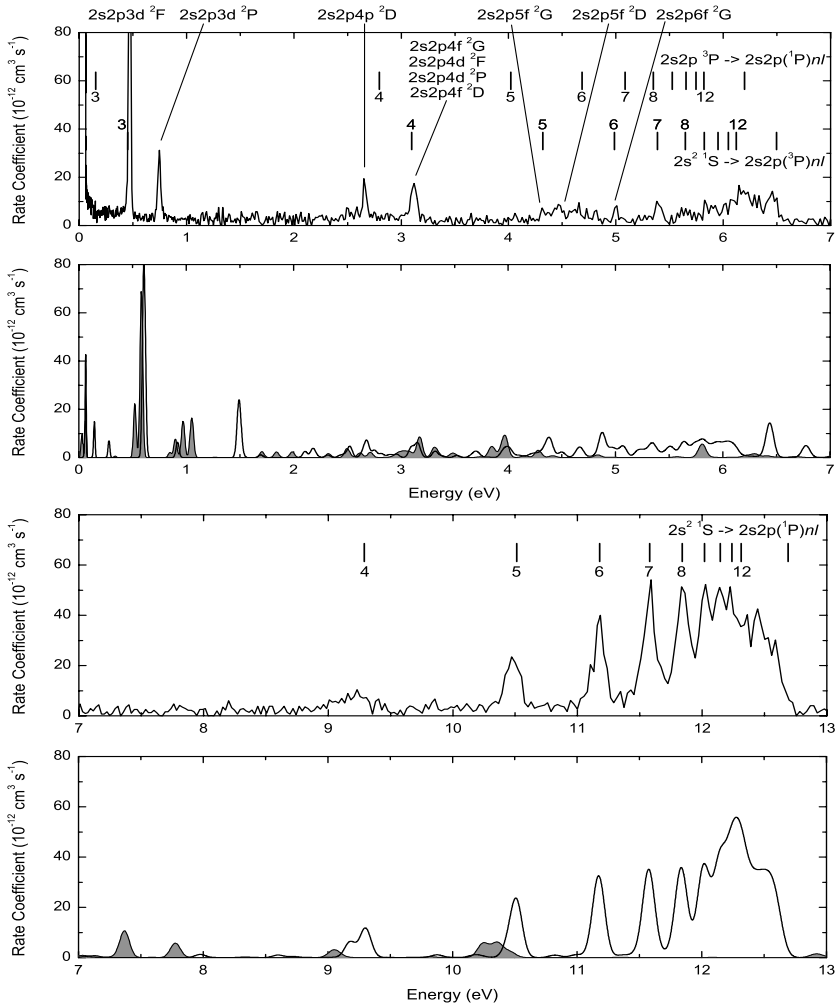

Fig. 1. The experimental DR recombination rate coefficient for C^{2+} (1st and 3rd plots). The energy positions of the $2s^2\,{}^1S \rightarrow 2s2p(^1P)nl$, $2s^2\,{}^1S \rightarrow 2s2p(^3P)nl$, and $2s2p\,{}^3P \rightarrow 2s2p(^1P)nl$ Rydberg series are shown for comparison. Also the AUTOSTRUCTURE results for the default calculation (solid lines in 2nd and 4th plots), and the results from the large configuration interaction calculation (shaded lines in 2nd and 4th plots) are shown. Note that both theory results are for the ground and metastable mixture specified in the text.

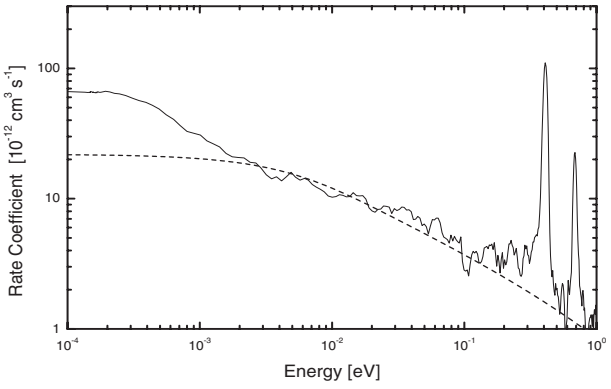

Fig. 2. The experimental RR rate coefficient for C^{2+}. The RR rate coefficient determined from Eq. (3), up to $n-$cutoff = 12 is illustrated by the dashed curve.

where v is the mean electron velocity and $f(\hat{v}, \boldsymbol{v})$ is the flattened Maxwellian velocity distribution of the electrons in the electron cooler. The RR cross section to a specific n is given by Kramers (1923)

$$\sigma_n^{\mathrm{RR}} = 2.105 \times 10^{-22}\,\Gamma\,\frac{Z^4\mathrm{R}^2}{nE(n^2E + Z^2\mathrm{R})}, \tag{4}$$

where Γ is the Gaunt factor taken from Seaton(1959), Z is the charge, and E is the incident electron energy. The RR rate coefficient, resulting from Eq. (3), for C^{2+} is shown in Fig. 2 (dashed curve). This RR rate coefficient is calculated from the lowest available principal quantum state, accounting for the number of vacancies, up to $n-$cutoff = 12. We will use this calculated RR rate coefficient to separate the RR and DR results when creating temperature dependent plasma rate coefficients, thereby avoiding the experimental RR enhancement. A separate RR calculation is made up to $n = 1000$ for the plasma rate coefficient.

The total temperature dependent plasma DR Maxwellian rate coefficient is determined from

$$\alpha\,(T_\mathrm{e}) = \int \alpha\,(E)\;f\,(E, T_\mathrm{e})\;\mathrm{d}E \tag{5}$$

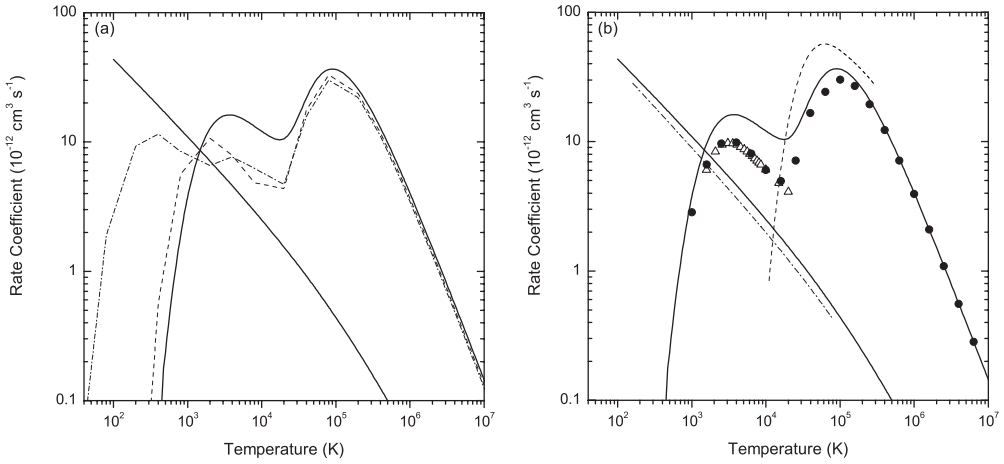

Fig. 3. The RR and DR Maxwellian plasma rate coefficients for C^{2+}. The RR from Eq. (3) up to $n = 1000$ and the hybrid calculation are given by the solid lines in both **a)** and **b)**, the default AUTOSTRUCTURE calculation by the dashed line in (a), and the large CI AUTOSTRUCTURE calculation by the dot-dashed line in **a)**. **b)** shows the current results compared to values from literature. The triangles show the low temperature DR results of Nussbaumer & Storey (1983), the filled circles show the DR results of Badnell (1987, 1988), the dashed line shows the DR results from Aldrovandi & Péquignot (1973), and the dot-dashed line represents the RR results of Péquignot et al. (1991).

where $\alpha(E)$ is the energy dependent rate coefficient and

$$f(E, T_e) = \frac{2E^{1/2}}{\pi^{1/2}(k_B T_e)^{3/2}} \exp\left(-\frac{E}{k_B T_e}\right), \quad (6)$$

is a Maxwellian distribution, where E is the energy and T_e is the mean electron temperature. Using Eq. (5), we have determined three sets of total DR plasma rate coefficients, shown in Fig. 4a. These plasma rate coefficients are i) the default AUTOSTRUCTURE total DR Maxwellian rate, which only has shifts of the NIST core excited energies (dashed line), ii) the large configuration interaction AUTOSTRUCTURE calculation for the $n = 3$ and 4 resonances, with the default AUTOSTRUCTURE results being used for the higher resonances (dot-dashed line), and iii) the hybrid experimental-theoretical total DR rate coefficient, where the ground state resonances have been isolated in the experiment, and the AUTOSTRUCTURE results are used for n-shells above the n-cutoff (solid line). Each of these DR Maxwellian rate coefficients are for the ground level total DR only.

In our hybrid Maxwellian rate coefficient, we account for the experimental n-cutoff using the default AUTOSTRUCTURE calculation to extrapolate the series limits above the n-cutoff to $n = 1000$. This requires matching the AUTOSTRUCTURE results to the experiment for higher n-shell resonances. The AUTOSTRUCTURE calculations are carried out assuming a 100% ion beam fraction for each initial state; ground or metastable. These are then scaled by the experimental ion beam metastable fraction, estimated at 60% metastable and 40% ground state for C^{2+}. The metastable fraction was primarily determined by the factor necessary to fit the $^1S - {}^1P$ theory to experiment in the series limit region. This metastable fraction determination is also supported by a separate electron-impact ionization measurement, maintaining the same ECR source parameters, Loch et al. (2005), which was performed in conjunction with this recombination measurement. In making a 100% ground state hybrid rate coefficient, the metastable components must be removed from the experimental data and the ground state components must be increased to reflect an adjustment from the 40% ground state fraction to 100%; simply by dividing by the determined ground state fraction. The four larger resonances in the 0–3.5 eV range are all identified to be from the initial ^1S ground state configuration. This is then combined with the remainder of the experimental rate coefficient at larger energies, also adjusted, minus the ^3P–^1P metastable contribution, and extrapolated to $n = 1000$ with the 100% ground state default AUTOSTRUCTURE calculation. Finally, this is convoluted to create the plasma rate coefficient given by the solid curve in Fig. 4.

It can be seen from Fig. 4 that the default AUTOSTRUCTURE data is reasonably close to the hybrid Maxwellian DR rate coefficient, while the large configuration interaction calculation, while agreeing at temperatures above 10^5 K, is significantly different at lower temperatures. Thus, it appears that including only the core excited energy shifts reproduces the experimental total DR rate reasonably well. This is reflected in the resonance results of Fig. 1. The small resonance near 0.02 eV, in the large configuration interaction calculation, is dominating the total DR rate coefficient at low temperatures, driving it away from the hybrid results. It is likely that the large configuration interaction calculation is not converged. These *nl* resonances are very slow to converge in the configuration interaction expansion, and it may be that we need to promote from the 1s subshell as well as the 2s and 2p, in order to achieve convergence. However, with the calculation we performed, we were already at the limits of our computational resources, due to the size of the calculation increasing rapidly with the number of configurations included. Thus, it may be that with more computational resources, a converged calculation could be achieved. Note that similar difficulties exist in achieving a converged calculation for N^{3+} and O^{4+}.

A detailed comparison of the default AUTOSTRUCTURE data with previous calculations has already been given in Colgan et al. (2004b), and so we make some brief comparisons

Table 1. Fit parameters to Eq. (7) for the C^{2+} pure ground state plasma DR rate coefficient in Fig. 3. The fit results are accurate to within 1% above 800 K.

i	c_i (cm^3 s^{-1} K$^{3/2}$)	E_i (eV)
1	1.12×10^{-5}	0.39
2	2.14×10^{-5}	1.33
3	3.77×10^{-5}	3.25
4	4.40×10^{-3}	12.05

Table 2. Fit parameters to Eq. (7) for the N^{3+} pure ground state plasma DR rate coefficient in Fig. 6 . The fit results are accurate to within 1% above 800 K.

i	c_i (cm^3 s^{-1} K$^{3/2}$)	E_i (eV)
1	4.22×10^{-6}	0.23
2	4.80×10^{-5}	0.69
3	1.93×10^{-4}	2.92
4	7.14×10^{-3}	14.83

with prominent RR and DR rate coefficients from the literature; plotted in Fig. 3b. We compare with the RR results of Péquignot et al. (1991), the LS-coupling low temperature DR rate coefficients of Nussbaumer & Storey (1983) (N&S), the DR rate coefficients of Badnell (1987, 1988), and the DR rate coefficients of Aldrovandi & Péquignot (1973). Given that we are primarily focused on the low energy resonances, and hence low temperatures, we will only make more detailed comparisons to the low temperature DR results of N&S.

Note that N&S used observed resonance energies for the recombined system in their calculation. The temperature validity range of 1580–23 000 K is used for comparison. The lower temperature is indicated by N&S to be where their calculated low temperature DR rate coefficient becomes unreliable. The higher temperature is where their calculated rate coefficient becomes greater than high temperature DR (as given by the Burgess (1964) formula). The N&S DR rate coefficient lies just between the hybrid pure ground state and experimental metastable fraction Maxwellian rate coefficients, and would need to be increased by ∼70% to be brought into agreement with the pure ground state hybrid Maxwellian rate coefficient in Fig. 4.

The pure ground state hybrid DR plasma rate coefficient in Fig. 3 is fitted by the expression

$$\alpha(T_\mathrm{e}) = T_\mathrm{e}^{-3/2} \sum_i c_i \exp\left(-\frac{E_i}{k_\mathrm{B} T_\mathrm{e}}\right) \quad (7)$$

where c_i and E_i are respectively related to the oscillator strength and the excitation energy. These values are given in Table 1 and reproduce the pure ground state hybrid DR plasma rate coefficient to within 1% above 800 K. The raw hybrid Maxwellian DR rate coefficient data, and these associated fitting coefficients represent our recommended total DR rate coefficient for C^{2+}.

Thus, our conclusion for C^{2+} DR is that the archived AUTOSTRUCTURE data is reasonably close to our best experimentally derived total rate coefficient. It was found that the low temperature default AUTOSTRUCTURE calculation is more accurate than the large configuration interaction AUTOSTRUCTURE calculations we performed.

4.2. $N^{3+} + e^- \rightarrow N^{2+}$

The N^{3+} experimental total recombination rate coefficient is shown in Fig. 4 along with the energy positions of the $^1S - {}^1P$, $^1S - {}^3P$, and $^3P - {}^1P$ Rydberg series detemined from Eq. (1) with respective E_s values of 16.2, 8.3, and 7.9 eV. The n-cutoff from Eq. (2) is 15. The calculated RR rate coefficient in Fig. 5 is carried out up to this cutoff for comparison with the experimental RR rate coefficient. The metastable ion beam fraction is estimated to be 40%. This is determined from the factor necessary to fit the $^1S - {}^1P$ theory to the experiment in the series limit region (60%). A small shift of −0.1 eV was necessary in the theory to align with the experimental rate coefficient near the $^1S - {}^1P$ series limit. This should, however, have a negligible effect on the plasma rate coefficient.

The resonance at 4.2 eV in Fig. 4 is identified, from the NIST levels database, to be the triply excited $2p^2(^3P)3p\ ^2D^o$ continuum state in N^{2+}, which suggests that this is a TR resonance. This resonance is comparatively small and negligible with regards to the plasma rate coefficient, however, it is intriguing to note that of the other Be-like ions studied, here and elsewhere, it seems that this is the first ion in the Be isoelectronic sequence which has an observable TR contribution.

The plasma total recombination reaction rate coefficients are determined in the same manner as C^{2+}. As for C^{2+}, the AUTOSTRUCTURE results agree poorly with the experimental resonances below 3 eV, of which all the prominent resonances result from an initial ground state configuration. These resonances are increased to reflect a 100% ground state and used in conjunction with the remaining extrapolated data, minus the metastable contribution, to create the pure ground state hybrid Maxwellian plasma rate coefficient. The resulting RR and DR plasma rate coefficients are given in Fig. 6.

We note that the low temperature differences in our various results are larger than those for the C^{2+} case. Again, the default AUTOSTRUCTURE calculation is actually closer to the hybrid calculation than the large AUTOSTRUCTURE configuration interaction calculation. Thus, the archived AUTOSTRUCTURE data of Colgan et al. (2004b) can be considered to be of reasonable quality above 0.8 eV, and starts to differ from the hybrid calculation at temperatures below that. The pure ground state hybrid Maxwellian plasma rate coefficient for N^{3+} in Fig. 6 is fitted with Eq. (7). The fit results are listed in Table 2. These values reproduce the pure ground state DR plasma rate coefficient to within 1% above 800 K

As for C^{2+}, we have plotted comparisons in Fig. 6b to results from the literature, however, we only mention the comparisons relevant to low temperature DR data. The low temperature plasma rate coefficient of N&S has a valid temperature range of 2510–36 000 K. This DR Maxwellian rate coefficient is about a factor of 1.5 less than the pure ground state hybrid Maxwellian DR rate coefficient and agrees best after being shifted down in temperature by ∼30%.

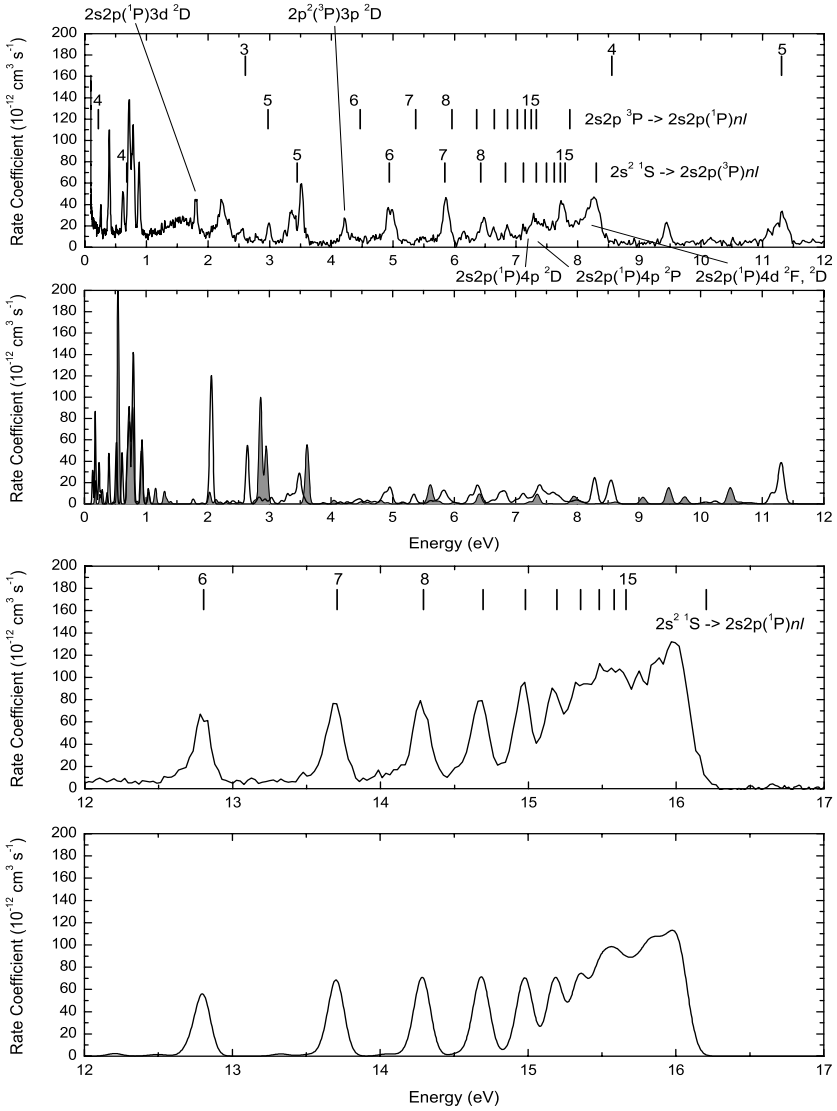

Fig. 4. The experimental DR recombination rate coefficient for N^{3+} (1st and 3rd plots). The $2s^2\ ^1S \rightarrow 2s2p(^1P)nl$, $2s^2\ ^1S \rightarrow 2s2p(^3P)nl$, and $2s2p\ ^3P \rightarrow 2s2p(^1P)nl$ Rydberg series are shown for comparison. The line types are the same as for Fig. 1.

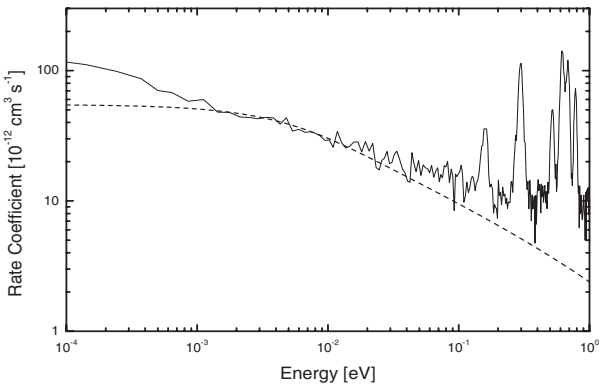

Fig. 5. The experimental RR rate coefficient for N^{3+}. The RR rate coefficient determined from Eq. (3) up to $n-$cutoff = 15 is illustrated by the dashed curve.

4.3. $O^{4+} + e^- \rightarrow O^{3+}$

The O^{4+} experimental DR rate coefficient is shown in Fig. 7 along with the energy positions of the $^1S - {}^1P$, $^1S - {}^3P$, and $^3P - {}^1P$ Rydberg series detemined from Eq. (1) with respective E_s values of 19.7, 10.2, and 9.5 eV. The n-cutoff from Eq. (2) is 17. The calculated RR rate coefficient in Fig. 8 is carried out up to this cutoff. The metastable ion beam fraction is estimated to be 35%. This is determined from the factor necessary to fit the $^1S - {}^1P$ theory to the experiment in the series limit region (65%).

Figure 7 has several identifiable TR resonances which are listed in Table 3 and marked in Fig. 7 by vertical short dashed lines. The first of these is a large freestanding resonance at 60 meV; best seen in Fig. 8. This resonance has a dramatic effect on the plasma rate coefficient, making resonant recombination larger than RR at temperatures well below 200 K.

The plasma Maxwellian rate coefficients are determined in the same manner as for C^{2+} and N^{3+}. The pure ground state hybrid Maxwellian rate coefficient is also made in the same fashion; by increasing the experimental resonances, minus any $^3P - {}^1P$ contributions, to reflect a 100% ground state and extrapolating with the 100% ground state AUTOSTRUCTURE

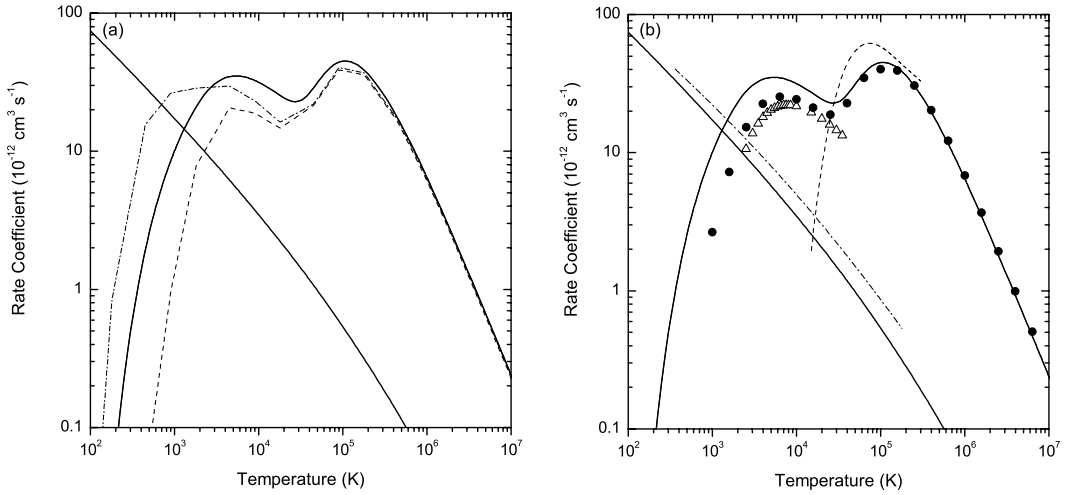

Fig. 6. The RR and DR maxwellian rate coefficients for the ground state of N^{3+}. Symbols and line types are the same as for Fig. 3.

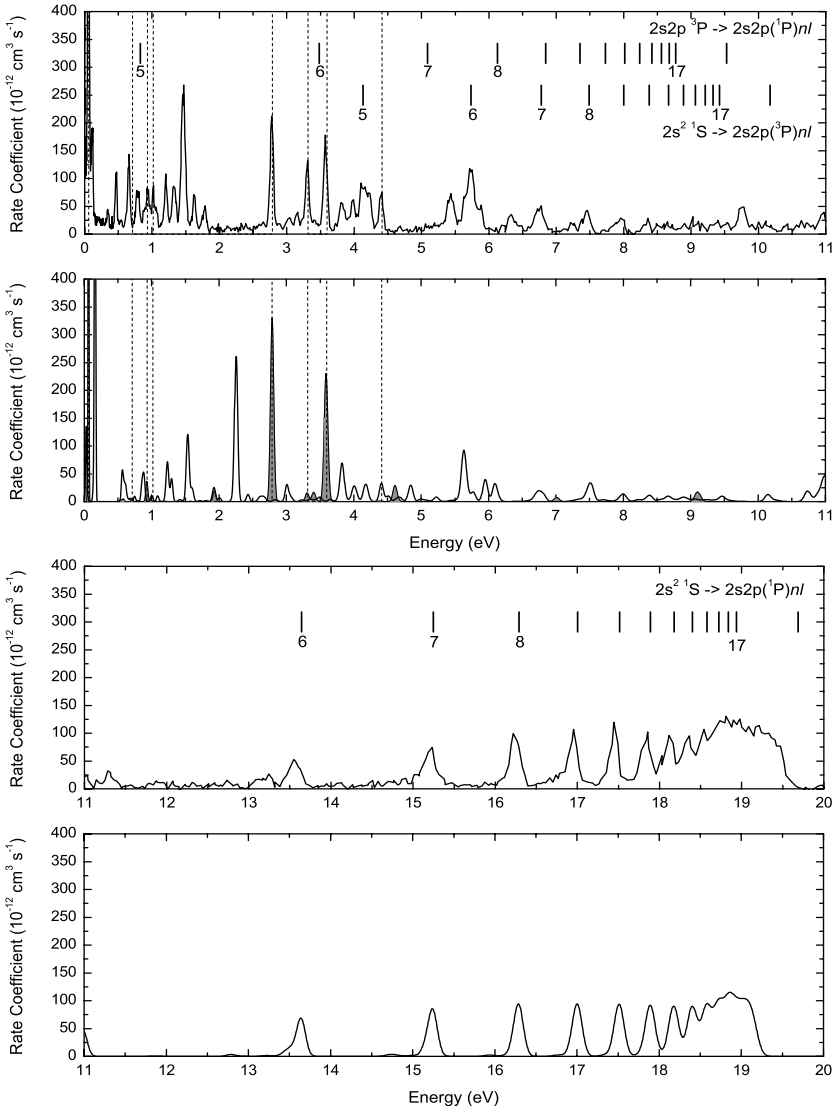

Fig. 7. The experimental DR recombination rate coefficient for O^{4+} (1st and 3rd plots). The energy positions of the 2s^2 ^{1}S $\rightarrow$ 2s2p(^{1}P)*nl*, 2s^2 ^{1}S $\rightarrow$ 2s2p(^{3}P)*nl*, and 2s2p ^{3}P $\rightarrow$ 2s2p(^{1}P)*nl* Rydberg series are shown for comparison. The vertical short dashed lines indicate the TR resonances predicted from the NIST data in Table 3. The remaining line types are the same as for Fig. 1.

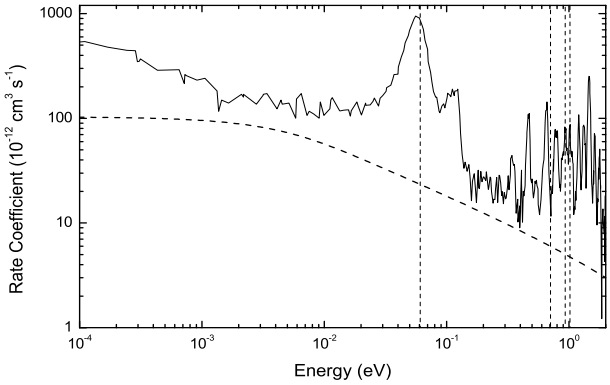

Fig. 8. The experimental RR rate coefficient for O^{4+}. The RR rate coefficient determined from Eq. (3) up to $n-$cutoff = 17 is illustrated by the dashed curve. The vertical short dashed lines indicate the low energy TR resonances predicted from the NIST data in Table 3.

Table 3. TR resonances observed in the O^{4+} experimental DR rate coefficient. Identification was made using the NIST levels database. The experimental resonance positions along with NIST predicted energy positions are listed with each state.

State	Resonance position (eV)	NIST energy (eV)
$2p^2(^1D)3p\ ^2F^o$	0.06	0.06
$2p^2(^3P)3d\ ^2F$	0.66	0.71
$2p^2(^1D)3p\ ^2D^o$	0.93	0.93
$2p^2(^3P)3d\ ^2P$	1.02	1.02
$2p^2(^3P)3d\ ^2D$	2.78	2.79
$2p^2(^1D)3d\ ^2F$	3.31	3.32
$2p^2(^1D)3d\ ^2D$	3.57	3.60
$2p^2(^1D)3d\ ^2P$	4.41	4.42

calculation. Since the previously mentioned TR resonances also initiate from the ^1S ground state, they are naturally included in this adjustment. In Fig. 9 we compare the plasma rate coefficients, using different approximations. The dashed curve in Fig. 9a shows the theory results, using energy shifts of the recombining system. The dashed-dotted curve in Fig. 9a shows the large configuration interaction calculation with resonance position shifts for the recombined system included for the low energy resonances. The solid curve represents our hybrid calculation. Note that the theory results, with only the shifts applied to the energies of the recombining system lies quite close to the hybrid result, implying that the archived data with only these shifts is reasonably accurate at low temperatures. This is because the theory result with only these core excited shifts, gets the resonance at 60 meV reasonably well. However, this is rather fortuitous, as it is clear from the resonance plot that it doesn't get other resonance positions to the same accuracy. The importance of the large TR resonance at 60 meV can be seen from the dotted curve results in Fig. 9a, where the large TR resonance has been artificially removed in the calculation of the Maxwellian rate coefficient. Thus, this large TR resonance effectively shifts the crossing point, where resonant recombination becomes larger than RR, to a much lower temperature.

Again, the total DR Maxwellian rate coefficients from the default AUTOSTRUCTURE calculation have already been compared to those existing in the literature by Colgan et al. (2004b). Thus, we concentrate on comparisons with data valid at low temperatures. The low temperature DR Maxwellian rate coefficient of N&S has a valid temperature range of 1000–46 000 K. The lower temperature is given explicitly by N&S for O^{4+}, due to insufficient reliability of their calculations. N&S point out that the predominant radiative decay channel of the $2p^2(^1D)3p\ ^2F^o$ state, responsible for the large TR resonance at 60 meV, is to the $2s2p^2\ ^2D$ state. The oscillator strength for this transition was calculated by their atomic structure code, in LS coupling, to be approximately three times larger than that determined from a close coupling calculation, due to the inclusion of configuration interaction in the close coupling method. N&S have used the oscillator strength from the close coupling calculation in determining their rate coefficient of O^{4+}.

Table 4. Fit parameters to Eq. (7) for the O^{4+} pure ground state plasma DR rate coefficient in Fig. 9 . The fit results are accurate to within 1% above 250 K and <5% between 100–250 K.

i	c_i (cm^3 s^{-1} K$^{3/2}$)	E_i (eV)
1	2.02×10^{-7}	0.01
2	1.51×10^{-5}	0.06
3	5.20×10^{-5}	0.54
4	3.46×10^{-4}	2.24
5	6.77×10^{-4}	6.93
6	4.09×10^{-3}	15.67
7	6.76×10^{-3}	21.28

The pure ground state hybrid Maxwellian plasma rate coefficient is fitted by Eq. (7) and the fit coefficients are given in Table 4. This fit reproduces that pure ground state rate coefficient to within 1% above 250 K and to within <5% between 100–250 K. Thus, our conclusions for O^{4+} are again that the archived AUTOSTRUCTURE data is of reasonable accuracy, and is close to the hybrid Maxwellian DR rate coefficient from this experiment. We find the presence of some very large TR resonance features, with one at 60 meV dominating the total DR Maxwellian rate coefficient at low temperatures.

5. Conclusion

The absolute RR and DR (TR) rate coefficients for Be-like C, N, and O have been measured using the CRYRING storage ring. In particular, these measurements have investigated low energy resonances which contribute to the rate coefficient and, ultimately, to the plasma Maxwellian rate coefficient.

Trielectronic recombination resonances have been observed in both N^{3+} and O^{4+}, with the later exhibiting several strong TR resonances. The TR contribution in O^{4+} has a dramatic effect on the plasma rate coefficient at low temperatures.

The temperature dependent Maxwellian plasma rate coefficients are determined by convoluting the experimental energy dependent rate coefficients with Maxwellian distributions for temperatures ranging from 10^2–10^7 K. The experimental metastable fraction is considered and field ionization induced n-cutoff is extrapolated using the AUTOSTRUCTURE routine.

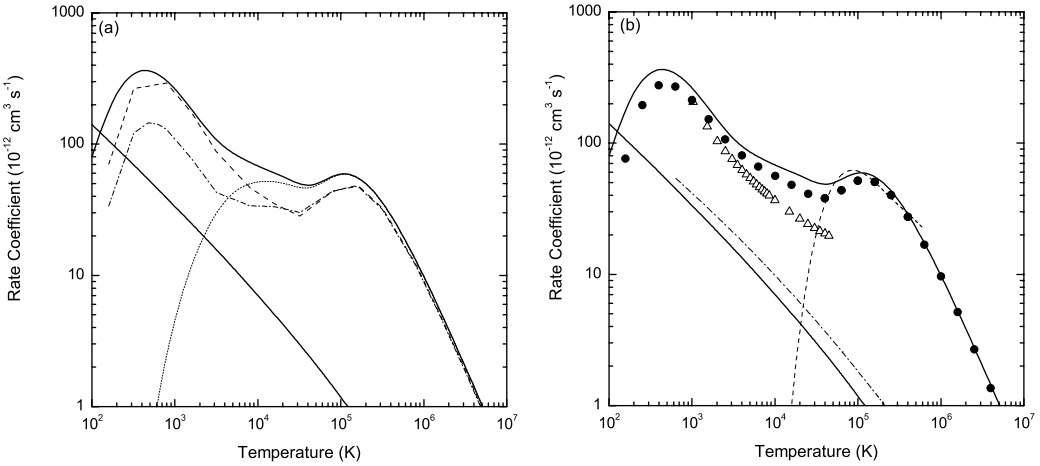

Fig. 9. The RR and DR plasma rate coefficients for O^{4+}. The dotted line in **a)** represents the hybrid calculation with the large TR resonance at 60 meV removed. The remaining line types and symbols are the same as for Fig. 3.

The resulting RR and DR plasma rate coefficients have been compared to the archived AUTOSTRUCTURE data of Colgan et al. (2004b), representing our default AUTOSTRUCTURE calculation, and to various rate coefficients from the literature. For each ion, we find that the archived data gives the closest agreement to the Maxwellian rates we construct from the experimental measurements. We find that performing larger AUTOSTRUCTURE configuration interaction calculations is not sufficient to provide any improvement in the low energy resonances for any of the ions studied, most likely because the large configuration interaction calculation has not converged. The experimental Maxwellian DR rate coefficients presented here offer an new basis for judging the applicability of existing Maxwellian DR rate coefficients in atomic databases, and in the literature.

Acknowledgements. M.F., P.G., S.M., and R.S. would like to acknowledge the Swedish Research Council for financial support. We are also grateful for the assistance received from the CRYRING staff at Manne Siegbahn Laboratory. S.L. and M.P. would like to acknowledge support by a grant for theoretical research in plasma and fusion science (DE-FG02-96ER54348) and a grant for scientific discovery through advanced computing (DE-FG02-01ER54644) to Auburn University by the US Department of Energy.

References

Altun, Z., Yumak, A., Badnell, N. R., Colgan, J., & Pindzola, M. S. 2004, A&A, 420, 775
Aldrovandi, S. M. V., & Péquignot, D. 1973, A&A, 25, 137
Aldrovandi, S. M. V., & Péquignot, D. 1976, A&A, 47, 321
Badnell, N. R. 1986, J. Phys. B, 19, 3827
Badnell, N. R. 1987, J. Phys. B: At. Mol. Opt. Phys., 20, 2081
Badnell, N. R. 1988, J. Phys. B: At. Mol. Opt. Phys., 21, 749
Badnell, N. R., Pindzola, M. S., Andersen, L. H., et al. 1991, J. Phys. B: At. Mol. Opt. Phys., 24, 4441
Badnell, N. R., O'Mullane, M. G., Summers, H. P., et al. 2003, A&A, 406, 1151
Burgess, A. 1965, ApJ, 141, 1588
Colgan, J., Pindzola, M. S., & Badnell, N. R. 2004a, A&A, 417, 1183
Colgan, J., Pindzola, M. S., Whiteford, A. D., & Badnell, N. R. 2004b, A&A, 412, 597
DeWitt, D. R., Schuch, R., Gao, H., et al. 1996, Phys. Rev. A, 53, 2327
Dittner, P. F., Datz, S., Krause, H. F., et al. 1987, Phys. Rev. A, 36, 33
Gao, H., DeWitt, D., Schuch, R., et al. 1995, Phys. Rev. Lett., 75, 4381
Kaler, J. B. 1981, ApJ, 249, 201
Kholtygin, A. F. & Feklistova, T. 1992, Baltic Astron., 1, 514
Kramers, H. A. 1923, Philos. Mag., 46, 836
Laughlin, C. A. 1980, Phys. Lett. A, 75, 199
Liu, X.-W. 2002, Rev. Mex. Astron. Astrofis., 12, 70
Loch, S. D., Witthoeft, M., Pindzola. M. S., et al. 2005, Phys. Rev. A, 71, 012716
Mitnik, D. M., & Badnell, N. R. 2004, A&A, 425, 1153
Müller, A. & Wolf, A. 1997, in Accelerator-based atomic physics techniques and applications, ed. J. C. Austin & S. M. Shafroth (Woodbury: AIP Press), 147
Nussbaumer, H. & Storey, P. J. 1983, A&A, 126, 75
Seaton, M. J. 1959, MNRAS, 119, 81
Schippers, S. 1999, Phys. Scr. T, 80, 158
Schippers, S., Müller, A., Gwinner, G., et al. 2001, ApJ, 555, 1027
Schnell, M., Gwinner, G., Badnell, N. R. et al 2003, Phys. Rev. Lett., 91, 043001
Schuch, R. 1993, in Review of Fundamental Processes and Applications of Atoms and ions, ed. C. D. Lin (Singapore: World Scientific), 169
Péquignot, D., Petitjean, P., & Boisson, C. 1991, A&A, 251, 680
Zatsarinny, O., Gorczyca, T. W., Korista, K. T., Badnell, N. R., & Savin, D. W. 2003, A&A, 412, 587
Zatsarinny, O., Gorczyca, T. W., Korista, K. T., Badnell, N. R., & Savin, D. W. 2004a, A&A, 417, 1173
Zatsarinny, O., Gorczyca, T. W., Korista, K. T., Badnell, N. R., & Savin, D. W. 2004b, A&A, 426, 699
Zong, W., Schuch, R., Lindroth, E., et al. 1997, Phys. Rev. A, 56, 386